

README - Data: Emulating long-term weather-driven transportation earthworks deterioration models to support asset management

Keywords: Slope stability; Slope stability analysis; Numerical modelling; Statistical emulation; Gaussian processes; Deterioration; Earthworks; Geotechnical modelling; Infrastructure deterioration; Cut slopes; Cutting stability; Embankment slopes.

Dataset link: <https://doi.org/10.25405/data.ncl.22714831>.

Summary

This document provides metadata on the linked dataset which was used in the preparation of the [Helm *et al.* \(2024\)](#) publication in the Elsevier journal: *Transportation Geotechnics*.

The linked repository consists of:

- Experimental design data (Latin hypercube sample design)
- Laboratory and numerical model validation data and results
- Modelled pore pressure results at slope scale
- Highways and rail slope geometry data for the M4 motorway and Great Western Main Line railway in the UK between London and Bristol
- Laboratory data on the peak and residual shear strength of a number of overconsolidated high plasticity clays
- Field data on the permeability of London Clay
- Geotechnical model and emulator output data relating geometry and material properties to time to failure

Funding Information

- The linked publication and the modelling data herein were produced as an output of the [ACHILLES](#) project, a UK EPSRC programme grant (EP/R034575/1).
- The field data from the BIONICS embankment are outputs of the UK EPSRC BIONICS (EP/F013221/1) and iSMART (EP/K027050/1) grants.
- The field data from the Newbury cutting were funded by UK EPSRC grant numbers GR/R72341/01 and EP/F063482/1.
- In both cases, continued funding for monitoring was also provided by the [ACHILLES](#) programme grant.

Publication Reference:

Helm, P.R., Svalova, A., Morsy, A.M., Rouainia, M., Smith, A., El-Hamalawi, A., Wilkinson, D.J., Postill, H. & Glendinning, S. (2024). Emulating long-term weather-driven transportation earthworks deterioration models to support asset management. *Transportation Geotechnics*. 44: 101155. <https://doi.org/10.1016/j.trgeo.2023.101155>.

Dataset Reference:

Helm, P.R., Svalova, A., Morsy, A.M., Rouainia, M., Smith, A., El-Hamalawi, A., Wilkinson, D.J., Postill, H. & Glendinning, S. (2024). *Data: Emulating long-term weather-driven transportation earthworks deterioration models to support asset management*. Dataset. Newcastle University. <https://doi.org/10.25405/data.ncl.22714831>.

Contents

1	Notes	1
2	Data	3
2.1	Figure 1	3
2.2	Figure 2	3
2.3	Figure 3	5
2.4	Figure 4	5
2.5	Figure 5	6
2.6	Figure 6	8
2.7	Figure 7	8
2.8	Figure 8	9
2.9	Figure 9	11
2.10	Figure 10	12
2.11	Figure 11	13
2.12	Figure 12	14
2.13	Figure 13	15
2.14	Figure 14	16
2.15	Figure 15	17
2.16	Figure 16	18
	References	21

List of Tables

A	Fitting parameters adopted for FoS curves in Figure 11.	13
B	Adopted parameters for emulation and used to produce Figure 12.	14
C	Adopted parameters for emulation and used to produce Figure 16.	18

List of Figures

A	Schematic diagram of the modelled simple shear test.	7
---	--	---

1 Notes

Units:

The units in this document are based on the SI system and follow the recommendations in the 9th edition of the Bureau International des Poids et Mesures (BIPM, 2022). One exception to this is in the context of time, where, in this work, the year is routinely used as a unit of measurement and is defined as 365 days in length ($60 \times 60 \times 24 \times 365 = 31\,536\,000$ s).

Notation:

- Variables are in *italic font* *e.g.* A, x, ϕ *etc.*
- Constants and function names are in upright (roman) font *e.g.* π, \sin .
- Vectors are typeset in **bold font** and marked with an arrow *e.g.* \vec{N}_g .
- Matrices and arrays are typeset in upper-case **bold font** *e.g.* **M**.
- Subscripts and superscripts are italicised if they are variables, or are descriptive but only a single character *e.g.* c'_p, k^r (peak drained cohesion and relative permeability respectively).
- Subscripts and superscripts are typeset in upright (roman) font if they are words or abbreviations of words *e.g.* $c'_{\max}, k^{\text{ref}}$ (maximum value of drained cohesion and a reference permeability respectively).
- Subscripts and superscripts may also be separated by a space *e.g.* $c'_{p\max}$ which in this case represents the maximum value of peak drained cohesion.

Language:

This document is drafted using British English spellings, except for the figure captions which are in US English as this is how they were written in the original journal publication.

In this document cross references to, and descriptions of figures and tables in the cited publication use Arabic numerals, whereas cross references to figures and tables within this document use uppercase Latin script to avoid ambiguity.

Date of data collection <format YYYY-MM-DD>:

The geotechnical modelling was performed from approx. 2019-06-01 to 2020-06-01. Field data collection for the model validation was performed from approx. 2003-01-01 to 2019-06-01 and the statistical emulation was undertaken from approx. 2020-06-01 to 2020-12-31.

Geographic location of data collection:

- Geotechnical model data was produced at Loughborough University and Newcastle University. The statistical emulation was performed at Newcastle University.
- Cut slope field hydrological data monitoring site: An instrumented cut slope on the A34 near Newbury, Berkshire (Lat: 51.3778, Lon: -1.3632). See Figure 1 in the Smethurst *et al.* (2012) paper for details. The field data were derived by researchers at the University of Southampton. Contact Dr. J. Smethurst for details.
- Embankment field hydrological data monitoring site: Bionics embankment, Nafferton Farm, Horsley, Northumberland (Lat: 54.9868, Lon: -1.9011). Hughes *et al.* (2009); Glendinning *et al.* (2014). See Figure 8 in the Stirling *et al.* (2021) paper and Figure 17 in Morsy *et al.* (2023b) for details. The field data were derived by researchers at Newcastle University. Field data for the BIONICS embankment is also available from the following institutional repository Yu *et al.* (2021)

Information about funding sources that supported the collection of the data:

- The linked publication and the modelling data in the linked repository were produced as an output of the UK EPSRC programme grant ACHILLES (EP/R034575/1). The instrumentation and monitoring of the Bionics embankment were funded by the BIONICS (GR/S87430/01) and iSMART (EP/K027050/1) grants also by EPSRC.
- The instrumentation and earlier monitoring of the Newbury cutting site was funded by the UK EPSRC under grant numbers GR/R72341/01 and EP/F063482/1. Further monitoring was also funded by ACHILLES.

Other information:

- Note that there is a reference list at the end of this document.
 - Within this readme, dates are written as YYYY-MM-DD (and using the Gregorian Calendar).
-

2 Data

2.1 Figure 1

Caption: Figure 1: Diagram showing the workflow required to produce asset and network scale deterioration data by the emulator.

Filename: N/A.

Data file contents: N/A.

Figure 1 is a schematic workflow diagram and contains no numeric data and therefore no entry was created in the repository.

2.2 Figure 2

Caption: Figure 2: Latin hypercube design dimension vectors showing the samples for a) the model geometry number (see Figure 8); b) the peak frictional strength; c) the apparent cohesion at peak strength and d) the reference hydraulic conductivity value. The values are obtained on a unit interval $[0, 1]$ and are then scaled to the required range.

Filename: Fig 2.xlsx

Data file contents:

The data file contains one readme tab and four data tabs (Fig. 2a, Fig. 2b, Fig. 2c and Fig. 2d) corresponding to the four Latin hypercube design dimension vectors.

Column headers:

Latin hypercube sample number:	The element number, Y , in the LHS dimension vector (units: –).
Latin hypercube sample:	The sample value, X , in element, Y , used to derive the parameter value (units: –).
Scaled parameter value:	The sample value, X , scaled to the deterministic model input value (units: variable).
Slope Height [m]:	Slope height (units: m).
Slope Angle [cot theta]:	Slope angle (units: –).
Slope Angle [deg.]:	Shear angle (units: °).
Scaled parameter value:	Geometry number drawn from LHS (units: –).
Scaled parameter value [deg.]:	Peak friction angle drawn from LHS (units: °).
Scaled parameter value [kPa]:	Apparent peak cohesion drawn from LHS (units: kPa).
Scaled parameter value [m/s]:	Reference permeability drawn from LHS (units: m s^{-1}).

Data description, derivation and processing:

The data are stored as tables of Latin hypercube sample number (from 1 to 76), Latin hypercube sample value from the standard uniform distribution ($X \sim U(0, 1)$), scaled sample value for use as model input (or to derive model input) and in the case of tab Fig. 2a, a figure showing the relation between model geometry and scaled sample value.

The underlying data for this figure were produced using the Latin hypercube sample (LHS) design tool in the Python packages PyDOE and PyDOE2 (Baudin, 2013; Sjögren & Svensson, 2018). The adopted LHS design was for a four factor design (geometry number, N_g , peak friction angle, ϕ'_p , peak apparent cohesion, c'_p , and reference permeability, k^r) with N samples, where $N = 76$ and adopting the maximin criterion which maximizes the minimum distance between sample points, and places the point in a randomized location within its interval. Each of the four factors is allocated to a unique dimension of the hypercube and the samples in each dimension are generated on a unit interval $[0, 1]$. These samples were then scaled to derive the geotechnical model input parameters.

The scaling adopted for the four dimensions of the LHS (\mathbf{LHS}_i , where $i = 1, 2, 3, 4$) were as follows:

$$\vec{N}_g = \lceil \mathbf{LHS}_1 \times N \rceil \quad (1)$$

$$\vec{\phi}'_p = [(\phi'_{p\max} - \phi'_{p\min}) \times \mathbf{LHS}_2] + \phi'_{p\min} \quad (2)$$

$$\vec{c}'_p = [(c'_{p\max} - c'_{p\min}) \times \mathbf{LHS}_3] + c'_{p\min} \quad (3)$$

$$\vec{k}^r = \frac{(k^r_{\max})^{\mathbf{LHS}_4}}{(k^r_{\min})^{\mathbf{LHS}_4 - 1}} \quad (4)$$

where \vec{N}_g , $\vec{\phi}'_p$, \vec{c}'_p and \vec{k}^r are vectors of length N containing the N_g , ϕ'_p , c'_p and k^r values, $\phi'_{p\max} = 25.0^\circ$, $\phi'_{p\min} = 18.5^\circ$, $c'_{p\max} = 10.0 \text{ kPa}$, $c'_{p\min} = 3.0 \text{ kPa}$, $k^r_{\max} = 2.5 \times 10^{-8} \text{ m s}^{-1}$, and $k^r_{\min} = 1.45 \times 10^{-9} \text{ m s}^{-1}$. The calculation steps are also included in the spreadsheet. Note that $\lceil \cdot \rceil$ and $\lfloor \cdot \rfloor$ in eqn. 1 denote a ceiling function.

2.3 Figure 3

Caption: Figure 3: Conceptual slope processes and behavior modeled in this work; a) cut slopes; b) embankment slopes.

Filename: N/A.

Data file contents: N/A.

Figure 3 is a schematic slope diagram and contains no numeric data and therefore no entry was created in the repository.

2.4 Figure 4

Caption: Figure 4: Schematic strain softening behavior. a) cut slope models of natural over-consolidated high plasticity clay as used to produce emulator input data where the residual strength, ϕ'_r , is a function of the peak strength and assumed liquid limit $f(\phi'_p, LL)$; b) intermediate plasticity compacted clay fill with time dependent softening from the peak value to the normally consolidated peak strength / critical state value. The material properties are summarized in Table 1 and Table 2.

Filename: N/A.

Data file contents: N/A.

Figure 4 is a schematic diagram showing the adopted clay strain softening behaviour which contains no data and therefore no entry was created in the repository.

2.5 Figure 5

Caption: Figure 5: a) & b) Calibration of the stiffness model [36] against oedometer swelling data at differing assumed values of K_0 [29,54]; c) Constant vertical stress, simple shear test data for London Clay [55] compared to the deterministic geotechnical model adopting local strain softening (LSS); d) Biaxial test data model used to calibrate the nonlocal strain softening (NLSS) model [after 36]. Adopted parameters highlighted in blue.

Caption references: [29] is Hight *et al.* (2007); [36] is Postill *et al.* (2021); [54] is Apted (1977); [55] is Lau (1988).

Filename: Fig 5.xlsx

Data file contents:

The data file contains one readme tab and one data tab (Fig. 5c) corresponding to the stated figure part, however note that the data for Fig. 5a, 5b and 5d are available from a separate dataset (Helm *et al.*, 2021).

Column headers:

Shear Strain [%]: Simple shear strain (units: %).

Shear Stress [kPa]: Shear stress (units: kPa).

Data description, derivation and processing:

The data for Fig. 5c is derived from simple shear test data produced by Lau (1988) and the modelled simple shear test data which was used to calibrate the strain softening model parameters. The data is formed of pairs of shear strain, ε_s (units: %) and shear stress, τ (units: kPa) for a range of confining vertical stresses (denoted as σ_v in the spreadsheet).

This calibration was undertaken in an element scale model test of simple shearing at a constant vertical stress where ε_s is derived from the horizontal displacement of the uppermost grid point of the element, u_x (units: m) and the element height, h_e (units: m). The horizontal displacement was driven by a constant horizontal velocity applied to the upper grid points of the model and the vertical stress is derived as a pressure applied to the upper model boundary. τ is derived from the horizontal reaction force, F_x (units: kN), acting on the face of the element with area, A_e (units: m²) as follows:

$$\varepsilon_s = \frac{u_x}{h_e} \times 100 \quad (5)$$

$$\tau = \frac{F_x}{A_e} \quad (6)$$

A schematic version of the modelled simple shear test is shown in Fig. A. The model base was fixed to prevent horizontal and vertical displacements, and the lateral boundaries were fixed to

prevent horizontal displacements. Note that in FLAC, displacement fixity conditions act on the zone corner grid points to prevent movements of the grid. However applied velocity boundary conditions in turn act on the fixity rather than the grid point (so the fixity moves at a constant velocity and the fixed grid point and hence model boundary is forced to move with it).

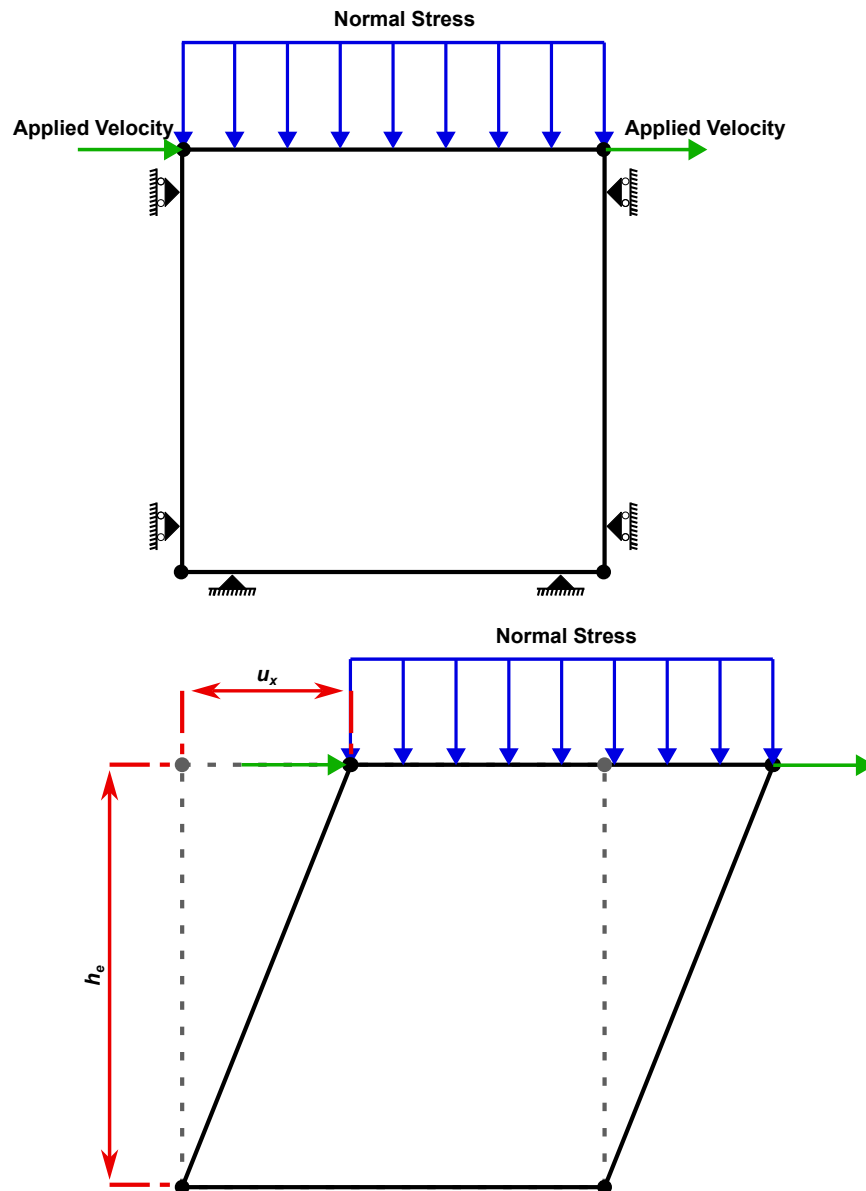


Figure A: Schematic diagram of the modelled simple shear test.

2.6 Figure 6

Caption: Figure 6: Validation of modeled cut slope hydrological behavior [36] against field tensiometer and piezometer data [56,57]; a) near surface behavior in the weathered London Clay; b) pore pressure cycles at greater depth in the lower permeability London Clay.

Caption References: [36] is Postill *et al.* (2021); [56] is Smethurst *et al.* (2006); [57] is Smethurst *et al.* (2012).

Filename: N/A.

Data file contents: N/A.

Figure 6 contains modelled pore water pressures that are available from a separate dataset (see Helm *et al.*, 2021). To request access to the field monitoring data, please contact the corresponding authors of Smethurst *et al.* (2006) and Smethurst *et al.* (2012) at Southampton University.

2.7 Figure 7

Caption: Figure 7: Validation of the embankment model; a) and c) modeled and laboratory undrained triaxial test data for the BIONICS embankment fill [after 34]; b) and d) modeled and laboratory undrained triaxial test data for the BIONICS embankment foundation soil [after 34]. e) and f) comparison of displacements derived using the current modeling approach to published vertical and horizontal displacements within an embankment [61].

Caption references: [34] is Morsy *et al.* (2023b); [61] is Clough & Woodward (1967).

Filename: N/A.

Data file contents: N/A.

Figure 7 contains validation data that are available from a separate dataset (see Morsy *et al.*, 2023a).

2.8 Figure 8

Caption: Figure 8: Percentage of cut slopes of varying geometries excavated into overconsolidated high plasticity (OC-HP) clays on a) the M4 motorway and b) the Great Western Main Line (GWML) railway between London and Bristol; c) the finalized geometry array from the experimental design showing the model numbers [after 64]. Slopes less than 3 m tall were excluded from the analyses.

Caption references: [64] is Svalova *et al.* (2021).

Filename: Fig 8.xlsx

Data file contents:

The data file contains one readme tab and three data tabs (Fig. 8a, Fig. 8b and Fig. 8c) corresponding to the three figure parts. Fig. 8a contains the highways slope data, Fig. 8b the railway data and Fig. 8c the data that relates geometry to model number (also see Fig. 2a).

Column headers:

Model Number:	The geometry and model number used to identify each of the deterministic geotechnical models. This matches the values plotted in Fig. 2a and Fig. 8c (units: –).
Slope Height [m]:	Slope height (units: m).
Slope Angle [cot theta]:	The adopted slope angle (units: –).
Slope Angle [deg.]:	The adopted slope angle (units: °).
Number of Slopes:	The number of slopes within the specified geometry bin (units: –).
% of Total:	The perc. of slopes within the specified geometry bin (units: –).
Road Slope:	Geometry bin contains specified slope type (units: –).
Rail Slope:	Geometry bin contains specified slope type (units: –).
Additional Slope:	Geometry bin contains specified slope type (units: –).

Data description, derivation and processing:

The data for Fig. 8a were derived from National Highways data passed to the research group by a member of our industrial advisory board. The highways slope geometry data are based on construction records and asset walk over surveys. The data were filtered to extract the overconsolidated clay cuttings, resulting in a total of 88 cutting slopes.

The data for Fig. 8b were derived from LiDAR scans of the rail corridor undertaken on behalf of Network Rail (2015 Network Rail National Aerial LiDAR Survey as described in Mellor *et al.*, 2017) and again provided by our industrial advisory board. For the LiDAR survey, LiDAR scans were undertaken at 20 m intervals along a given line (in this case the data from the Great Western Main Line between London Paddington Station and Bristol Temple Meads), with each scan performed along a section perpendicular to the railway, and extending 50 m to

either side. From each of these scans, and for each side of the railway the average slope height and slope angle was derived. It was this processed data that was provided to the research group. Where multiple scan section geometries were available for a given earthwork, a single slice was selected as representative of the worst case geometry based on a morphology factor, F_M :

$$F_M = H \tan(\theta) \quad (7)$$

where H is slope height (m) and θ is the slope angle (rad) and the largest F_M value was adopted as the assumed worst case geometry. It may also be worth noting that slopes on opposite sides of the line are given differing earthworks identification numbers and so were treated here as separate slopes (even though they would have been excavated as part of a single cut). The data was then filtered to extract only the cuttings excavated within high plasticity overconsolidated clays. This resulted in 365 cut slope geometries being defined for the railway between London and Bristol.

The highways and railway data were then binned based on their height and angle with the height bins centred at 2 m intervals from 4 m to 20 m and the angle bins centred at intervals of $\cot(\theta) = 0.5$ from $\cot(\theta) = 0.5$ ($\approx 63.5^\circ$) to $\cot(\theta) = 7.5$ ($\approx 7.5^\circ$). The counts of slopes within each bin were then used to derive the percentages as plotted in Figure 8a and 8b in the paper.

Fig. 8c summarises the model / geometry numbers, their relation to the respective slope geometry and the asset type they represent (road or rail cut slopes). The additional slope column represents slope geometries that were added to the LHS design in order to ensure there were sufficient deterministic model numbers and hence results to allow effective emulation to be undertaken.

2.9 Figure 9

Caption: Figure 9: a) Adopted peak strength envelope range for the modeling of overconsolidated high plasticity (OC-HP) clays; b) adopted hydraulic conductivity range and variation with depth.

Filename: Fig 9.xlsx

Data file contents:

The data file contains one readme tab and two data tabs (Fig. 9a and Fig. 9b) corresponding to the two figure parts. Fig 9a contains the peak shear strength data for the overconsolidated clays and Fig 9b contains the permeability data.

Column headers:

(sig_1+sig_3)/2 [kPa]:	Average effective stress (centre of Mohr circle, units: kPa).
(sig_1-sig_3)/2 [kPa]:	Maximum shear stress (radius of Mohr circle, units: kPa).
Hyd. Cond. [m/s]:	The hydraulic conductivity* (units: m s ⁻¹).
Depth [m]:	The depth below the ground surface (units: m).

*May be described as the coefficient of permeability elsewhere in the dataset.

Data description, derivation and processing:

The peak shear strength data for Fig. 9a were derived from a range of publications related to overconsolidated high plasticity (OC-HP) clays, specifically the sources summarised here: see Chandler (1972); Sandroni (1977); Apted (1977) and Cripps & Taylor (1987). The data are summarised as pairs of effective stress, σ' , and shear stress, τ , respectively:

$$\sigma' = \frac{(\sigma'_1 + \sigma'_3)}{2} \quad (8)$$

$$\tau = \frac{(\sigma'_1 - \sigma'_3)}{2} \quad (9)$$

where σ'_1 and σ'_3 are the maximum and minimum principal effective stresses respectively.

The permeability data for Fig. 9b were derived from a range of publications related to overconsolidated high plasticity (OC-HP) clays, specifically the sources summarised here: see Garga (1970); Dixon & Bromhead (1999); Gourvenec *et al.* (2005) and Dixon *et al.* (2019). The modelled permeability distributions were fitted using the relations outlined in the published paper (Helm *et al.*, 2024). Note that elements of this permeability dataset were previously made available in Helm *et al.* (2021) and used in the publication (Postill *et al.*, 2021).

2.10 Figure 10

Caption: Figure 10: The residual frictional strength range adopted in the modeling compared to laboratory and field data along with the residual strength adopted for overconsolidated high plasticity clays in other work.

Filename: Fig 10.xlsx

Data file contents:

The data file contains one readme tab and one data tab (Fig. 10). Fig. 10 contains the residual shear strength data for the overconsolidated clays.

Column headers:

sigma_n [kPa]:	Normal effective stress, σ'_n (units: kPa).
tan(phi_r):	Residual frictional strength, $\tan(\phi'_r)$, (units: –).
tau_r [kPa]:	The residual shear strength, τ_r (units: kPa).
phi_r [deg.]:	The residual frictional strength, ϕ'_r (units: °).
$(\bar{x} \pm sz) \times \text{sigma_n}$:	The strength range covered by 99 % confidence interval (units: kPa).
Max phi_r [deg]:	The maximum value of residual friction, $\phi'_{r \max}$ (units: °).
Min phi_r [deg]:	The minimum value of residual friction, $\phi'_{r \min}$ (units: °).

Data description, derivation and processing:

The residual shear strength data for Fig. 10 were derived from a range of publications related to overconsolidated high plasticity (OC-HP) clays, specifically the sources summarised here: see Lupini (1980); Lupini *et al.* (1981); Bromhead & Dixon (1986); Potts *et al.* (1997); Ellis & O'Brien (2007); and Rouainia *et al.* (2020).

The “typical range” of residual strength data plotted in Figure 10 is derived from the 99% confidence interval, CI, for the range of the Bromhead & Dixon (1986) residual friction data ($\bar{x} \approx 11.75^\circ$, $s \approx 1.5^\circ$, $z = 2.576$):

$$CI = \bar{x} \pm sz \quad (10)$$

where \bar{x} is the sample mean, s is the sample standard deviation and z is the z-score for 99% CI and the bounds of the residual shear strength envelope ($\tau_{r \min}$ and $\tau_{r \max}$) is given by:

$$\tau_{r \min}, \tau_{r \max} = (\bar{x} \pm sz) \times \sigma'_n \quad (11)$$

where σ'_n is normal effective stress.

2.11 Figure 11

Caption: Figure 11: Example factor of safety deterioration curves for a range of geometries and material parameters derived from the deterministic geotechnical models which used the Latin hypercube experimental design input parameters.

Filename: Fig 11.xlsx

Data file contents:

The data file contains one readme tab and one data tab (Fig. 11). The Fig. 11 tab contains the annual worst case factor of safety (FoS) output data from four slope models, all with angles of 1V in 3H, and with heights of 8 m, 10 m, 12 m and 16 m.

Column headers:

Time [years]: Time from start of model run (units: yr).

FoS [-]: Factor of safety against ultimate limit state shear failure (units: –).

Data description, derivation and processing:

For this plot, for each of the models, a curve was fitted with the following form:

$$\text{FoS} = \frac{\text{FoS}_{\max}}{\left[1 + \left(\frac{1}{a}t\right)^b\right]^{(1-1/b)}} \quad (12)$$

where FoS_{\max} is the maximum value of FoS, a and b are fitting parameters that control the point on the x-axis when FoS starts to decrease (yr), and the rate of decrease respectively and t is the time (yr). The adopted fitting parameters are summarised in Table A.

Table A: Fitting parameters adopted for FoS curves in Figure 11.

Model No. [-]	Slope Angle [Vert. in Hori.]	Slope Height [m]	FoS _{max} [-]	a [Years]	b [-]
36	1 in 3	8.0	1.91	129.97	4.79
45	1 in 3	10.0	1.88	107.43	5.76
52	1 in 3	12.0	1.84	95.00	8.00
63	1 in 3	16.0	1.90	80.96	7.54

2.12 Figure 12

Caption: Figure 12: Emulator output showing time to failure for varying cut slope geometries for specified strength and hydraulic conductivity; a) the minimum strength and maximum hyd. conductivity; b) the median of the properties; c) the maximum strength and minimum hydraulic conductivity, d) properties representative of London Clay as used in previous cut slope modeling studies [e.g. 36, 38].

Caption references: [36] is Postill *et al.* (2021); [38] is Rouainia *et al.* (2020).

Filename: Fig 12.xlsx

Data file contents:

The data file contains one readme tab and four data tabs (Fig. 12a, Fig. 12b, Fig. 12c, Fig. 12d), which contain the data used to plot the four parts of the relevant figure.

Column headers:

Slope Angle [cot theta]:	Slope angle (units: –).
Slope Height [m]:	Slope height (units: m).
Time to Failure [years]:	The time taken to reach failure from the end of cutting excavation (units: yr).

Data description, derivation and processing:

The raw emulator output gives slope angle, height and time to failure as columns of data. This was then re-gridded in Python using NumPy (Harris *et al.*, 2020) to create three 30×30 matrices, each containing one of the properties. These matrices were then passed to Matplotlib's (Hunter, 2007) `contourf` (filled contours) and `contour` (contour lines) functions with the specified contour intervals to create the plot. The co-ordinates of the contour lines were then exported. These data (i.e. the raw emulator output, the re-gridded data, and the coordinates of the contour lines) are available for each of the four property combinations of peak friction (ϕ'_p), apparent peak cohesion (c'_p) and reference hydraulic conductivity (k_h^{ref}) as listed in Table B.

Table B: Adopted parameters for emulation and used to produce Figure 12.

Figure Sub Plot	c' [°]	ϕ'_p [kPa]	k_h^{ref} [m/s]
Fig. 12a	3.00	18.50	2.5×10^{-8}
Fig. 12b	6.50	21.75	6.1×10^{-9}
Fig. 12c	10.00	25.00	1.5×10^{-9}
Fig. 12d	7.00	20.00	5.0×10^{-9}

The emulator code used to derive the raw output data has been made available via an open access license (Svalova, 2021) and is documented in Svalova *et al.* (2021).

2.13 Figure 13

Caption: Figure 13: Proportion of stable slopes of varying heights at angles of a) 1V in 2.0H; b) 1V in 2.5H; c) 1V in 3.0H; d) 1V in 3.5H as a function of time from end of construction. *N.B.* the times to failure for $P_f = 0.5$ are intended to aid comparison only and are not recommended design values.

Filename: Fig 13.xlsx

Data file contents:

The data file contains one readme tab and four data tabs (Fig. 13a, Fig. 13b, Fig. 13c, Fig. 13d), which contain the data used to plot the four parts of the relevant figure.

Column headers:

Time [years]:	Time in years at which a given percentage of the specified assets remain stable (units: yr).
1 – ECDF [%]:	Percentage of assets currently stable changing with time (units: %).

Data description, derivation and processing:

The raw emulator output is provided here as 1 – ECDF (where ECDF is the empirical cumulative distribution function) for a set of four differing slope angles (1V in 2.0H, 1V in 2.5H, 1V in 3.0H and 1V in 3.5H) each with a range of slope heights. Each set of 1 – ECDF data covers the full range of material properties. The emulator code used to derive this data has been made available open access (Svalova, 2021) and is documented in Svalova *et al.* (2021).

2.14 Figure 14

Caption: Figure 14: Proportion of stable slopes of varying slope angles at heights of a) 5 m; b) 10 m; c) 15 m; d) 20 m as a function of time from end of construction. NB the times to failure for a probability of 0.5 are intended to aid comparison only and are not recommended design values.

Filename: Fig 14.xlsx

Data file contents:

The data file contains one readme tab and four data tabs (Fig. 14a, Fig. 14b, Fig. 14c, Fig. 14d), which contain the data used to plot the four parts of the relevant figure.

Column headers:

Time [years]: Time in years at which a given percentage of the specified assets remain stable (units: yr).

1 – ECDF [%]: Percentage of assets currently stable changing with time (units: %).

Data description, derivation and processing:

The raw emulator output is provided here as 1 – ECDF (where ECDF is the empirical cumulative distribution function) for a set of four differing slope heights (5 m, 10 m, 15 m, 20 m) each with a range of differing slope angles and with each set of 1 – ECDF data covering the full range of material properties. The emulator code used to derive this data has been made available open access (Svalova, 2021) and is documented in Svalova *et al.* (2021).

2.15 Figure 15

Caption: Figure 15: Proportion of stable slopes with time for variations in the assumed properties; a) varying apparent cohesion; b) varying friction angle; c) varying reference hydraulic conductivity; d) variation in all material properties as per Table 3 and applied to the full range of slope geometries. The dashed curve represents the behaviour for typical London Clay properties. NB the times to failure for a probability of 0.5 are intended to aid comparison only and are not recommended design values.

Filename: Fig 15.xlsx

Data file contents:

The data file contains one readme tab and four data tabs (Fig. 15a, Fig. 15b, Fig. 15c, Fig. 15d), which contain the data used to plot the four parts of the relevant figure.

Column headers:

Time [years]:	Time in years at which a given percentage of the specified assets remain stable (units: years).
1 – ECDF [%]:	Percentage of assets currently stable changing with time (units: %).

Data description, derivation and processing:

The raw emulator output is provided here as 1 – ECDF (where ECDF is the empirical cumulative distribution function) and is intended to demonstrate the relative effect of each of the individual properties on the time to failure. The first three spread sheet tabs (a to c) cover variation in peak friction, apparent peak cohesion and reference permeability respectively and cover the full range of all other properties. The fourth tab (d) includes 1 – ECDF that covers a subset of each of the key material properties while covering the full range of cut slope geometries. The emulator code used to derive this data has been made available open access (Svalova, 2021) and is documented in Svalova *et al.* (2021).

2.16 Figure 16

Caption: Figure 16: The time to failure for differing slope geometries and asset types (highways vs rail) considering the range of adopted material properties of the London Clay, annotated with typical design life values and the current maximum age of UK railways slope infrastructure, a) lowest stability properties; b) mean properties; c) maximum stability properties.

Filename: Fig 16.xlsx

Data file contents:

The data file contains one readme tab and three data tabs (Fig. 16a, Fig. 16b, Fig. 16c), which contain the data used to plot the three parts of the relevant figure.

Column headers:

Slope Angle (cot theta): Slope angle (units: –).
 Time to Failure (years): The time taken to reach failure from the end of cutting excavation (units: yr).

Data description, derivation and processing:

The raw emulator output used to produce Figure 12 (see Fig 12.xlsx) was regridded and interpolated to give time to failure at higher resolutions of slope angle change (increased from $\cot(\theta) \approx 0.241$ to $\cot(\theta) = 0.01$) using NumPy in Python (Harris *et al.*, 2020). This was then plotted as slope angle vs time to failure for differing slope heights and material properties. The adopted properties used in Figure 16 are summarised in Table C.

Table C: Adopted parameters for emulation and used to produce Figure 16.

Figure Sub Plot	c' [°]	ϕ'_p [kPa]	k_h^{ref} [m/s]
Fig. 16a	3.00	18.50	2.5×10^{-8}
Fig. 16b	6.50	21.75	6.1×10^{-9}
Fig. 16c	10.00	25.00	1.5×10^{-9}

The slope geometry data for the differing transport infrastructure types (*i.e.* rail and road slope data from Fig. 8.xlsx) were then overlain onto the plots of slope angle vs time to failure data to illustrate the difference between the two types.

References

- Apted, J. P. (1977). *Effects of weathering on some geotechnical properties of London Clay*. Ph.D. thesis, Imperial College of Science and Technology, University of London, URL: <http://hdl.handle.net/10044/1/8897>.
- Baudin, M. (2013). pyDOE: The Experimental Design Package for Python - Randomized Designs. URL: <https://pythonhosted.org/pyDOE/randomized.html>.
- BIPM (2022). *The International System of Units (SI)*. 9th edn., Bureau International des Poids et Mesures. URL: <https://www.bipm.org/documents/20126/41483022/SI-Brochure-9-EN.pdf>.
- Bromhead, E. N. & Dixon, N. (1986). The field residual strength of London Clay and its correlation with laboratory measurements, especially ring shear tests. *Géotechnique* **36**, No. 3, 449–452, doi:10.1680/geot.1986.36.3.449.
- Chandler, R. J. (1972). Lias clay: weathering processes and their effect on shear strength. *Géotechnique* **22**, No. 3, 403–431, doi:10.1680/geot.1972.22.3.403.
- Clough, R. W. & Woodward, R. J. (1967). Analysis of embankment stresses and deformations. *Journal of the Soil Mechanics and Foundations Division* **93**, No. 4, 529–549, doi:10.1061/JSFEAQ.0001005.
- Cripps, J. C. & Taylor, R. K. (1987). Engineering characteristics of British over-consolidated clays and mudrocks, II. Mesozoic deposits. *Engineering Geology* **23**, No. 3-4, 213–253, doi:10.1016/0013-7952(87)90091-3.
- Dixon, N. & Bromhead, E. N. (1999). Depth-dependent permeability in London Clay measured using standpipe piezometer equilibration data. *Géotechnique* **49**, No. 5, 651–660, doi:10.1680/geot.1999.49.5.651.
- Dixon, N., Crosby, C. J., Stirling, R., Hughes, P. N., Smethurst, J., Briggs, K., Hughes, D., Gunn, D., Hobbs, P., Loveridge, F., Glendinning, S., Dijkstra, T. & Hudson, A. (2019). In situ measurements of near-surface hydraulic conductivity in engineered clay slopes. *Quarterly Journal of Engineering Geology and Hydrogeology* **52**, No. 1, 123–135, doi:10.1144/qjagh2017-059.
- Ellis, E. A. & O'Brien, A. S. (2007). Effect of height on delayed collapse of cuttings in stiff clay. *Proceedings of the Institution of Civil Engineers - Geotechnical Engineering* **160**, No. 2, 73–84, doi:10.1680/geng.2007.160.2.73.
- Garga, V. K. (1970). *Residual shear strength under large strains and the effect of sample size on the consolidation of fissured clay*. Ph.D. thesis, University of London (Imperial College of Science and Technology), UK, URL: <http://hdl.handle.net/10044/1/16399>.
- Glendinning, S., Hughes, P., Helm, P., Chambers, J., Mendes, J., Gunn, D., Wilkinson, P. & Uhlemann, S. (2014). Construction, management and maintenance of embankments used for road and rail infrastructure: implications of weather induced pore water pressures. *Acta Geotechnica* **9**, No. 5, 799–816, doi:10.1007/s11440-014-0324-1.
- Gourvenec, S. M., Mair, R. J., Bolton, M. D. & Soga, K. (2005). Ground conditions around an old tunnel in London Clay. *Proceedings of the Institution of Civil Engineers - Geotechnical Engineering* **158**, No. 1, 25–33, doi:10.1680/geng.2005.158.1.25.

- Harris, C. R., Millman, K. J., van der Walt, S. J., Gommers, R., Virtanen, P., Cournapeau, D., Wieser, E., Taylor, J., Berg, S., Smith, N. J., Kern, R., Picus, M., Hoyer, S., van Kerkwijk, M. H., Brett, M., Haldane, A., del Río, J. F., Wiebe, M., Peterson, P., Gérard-Marchant, P., Sheppard, K., Reddy, T., Weckesser, W., Abbasi, H., Gohlke, C. & Oliphant, T. E. (2020). Array programming with NumPy. *Nature* **585**, No. 7825, 357–362, doi:10.1038/s41586-020-2649-2.
- Helm, P., Postill, H., Dixon, N., Glendinning, S., Smethurst, J., Rouainia, M., Briggs, K., El-Hamalawi, A. & Blake, A. (2021). Data: Forecasting the long-term deterioration of a cut slope in high-plasticity clay using a numerical model. Dataset. Newcastle University, doi: 10.25405/data.ncl.19762144.
- Helm, P., Svalova, A., Morsy, A., Rouainia, M., Smith, A., El-Hamalawi, A., Wilkinson, D., Postill, H. & Glendinning, S. (2024). Emulating long-term weather-driven transportation earthworks deterioration models to support asset management. *Transportation Geotechnics* **44**, 101155, doi:10.1016/j.trgeo.2023.101155.
- Hight, D. W., Gasparre, A., Nishimura, S., Minh, N. A., Jardine, R. J. & Coop, M. R. (2007). Characteristics of the London Clay from the Terminal 5 site at Heathrow Airport. *Géotechnique* **57**, No. 1, 3–18, doi:10.1680/geot.2007.57.1.3.
- Hughes, P. N., Glendinning, S., Mendes, J., Parkin, G., Toll, D. G., Gallipoli, D. & Miller, P. E. (2009). Full-scale testing to assess climate effects on embankments. *Proceedings of the Institution of Civil Engineers - Engineering Sustainability* **162**, No. 2, 67–79, doi:10.1680/ensu.2009.162.2.67.
- Hunter, J. D. (2007). Matplotlib: A 2D graphics environment. *Computing in Science & Engineering* **9**, No. 3, 90–95, doi:10.1109/MCSE.2007.55.
- Lau, W. (1988). *The behaviour of clay in simple shear and triaxial tests*. Ph.D. thesis, City, University of London, URL: http://openaccess.city.ac.uk/8347/1/The_behaviour_of_clay_in_simple_shear_and_triaxial_tests.pdf.
- Lupini, J. F. (1980). *The residual strength of soils*. Ph.D. thesis, Imperial College of Science and Technology, University of London, URL: <http://hdl.handle.net/10044/1/11442>.
- Lupini, J. F., Skinner, A. E. & Vaughan, P. R. (1981). The drained residual strength of cohesive soils. *Géotechnique* **31**, No. 2, 181–213, doi:10.1680/geot.1981.31.2.181.
- Mellor, R., Parry, L., Power, C. & Spink, T. (2017). CP6 Earthworks Asset Policy Development Task 36 – Global Stability and Resilience Appraisal Interim Report. *Technical report*, Network Rail, Milton Keynes, UK.
- Morsy, A., Helm, P., El-Hamalawi, A., Smith, A., Hughes, P., Stirling, R., Dijkstra, T., Dixon, N. & Glendinning, S. (2023a). Data used for the validation of the BIONICS research embankment hydromechanical model. Dataset. Newcastle University, doi:10.25405/data.ncl.22144442.v1.
- Morsy, A. M., Helm, P. R., El-Hamalawi, A., Smith, A., Hughes, P. N., Stirling, R. A., Dijkstra, T. A., Dixon, N. & Glendinning, S. (2023b). Development of a multiphase numerical modeling approach for hydromechanical behavior of clay embankments subject to weather-driven deterioration. *Journal of Geotechnical and Geoenvironmental Engineering* **149**, No. 8, 04023062, doi:10.1061/JGGEFK.GTENG-11213.

- Postill, H., Helm, P., Dixon, N., Glendinning, S., Smethurst, J., Rouainia, M., Briggs, K., El-Hamalawi, A. & Blake, A. (2021). Forecasting the long-term deterioration of a cut slope in high-plasticity clay using a numerical model. *Engineering Geology* **280**, 105912, doi:10.1016/j.enggeo.2020.105912.
- Potts, D. M., Kovacevic, N. & Vaughan, P. R. (1997). Delayed collapse of cut slopes in stiff clay. *Géotechnique* **47**, No. 5, 953–982, doi:10.1680/geot.1997.47.5.953.
- Rouainia, M., Helm, P., Davies, O. & Glendinning, S. (2020). Deterioration of an infrastructure cutting subjected to climate change. *Acta Geotechnica* **15**, No. 10, 2997–3016, doi:10.1007/s11440-020-00965-1.
- Sandroni, S. S. (1977). *The Strength of London Clay in Total and Effective Stress Terms*. Doctoral thesis, Imperial College of Science and Technology, University of London, URL: <https://spiral.imperial.ac.uk/handle/10044/1/7682>.
- Sjögren, R. & Svensson, D. (2018). pyDOE2: An experimental design package for python. URL: <https://libraries.io/pypi/pyDOE2>.
- Smethurst, J. A., Clarke, D. & Powrie, W. (2006). Seasonal changes in pore water pressure in a grass-covered cut slope in London Clay. *Géotechnique* **56**, No. 8, 523–537, doi:10.1680/geot.2006.56.8.523.
- Smethurst, J. A., Clarke, D. & Powrie, W. (2012). Factors controlling the seasonal variation in soil water content and pore water pressures within a lightly vegetated clay slope. *Géotechnique* **62**, No. 5, 429–446, doi:10.1680/geot.10.P.097.
- Stirling, R. A., Toll, D. G., Glendinning, S., Helm, P. R., Yildiz, A., Hughes, P. N. & Asquith, J. D. (2021). Weather-driven deterioration processes affecting the performance of embankment slopes. *Géotechnique* **71**, No. 11, 957–969, doi:10.1680/jgeot.19.SiP.038.
- Svalova, A. (2021). Code for emulating computer experiments of infrastructure slope stability using Gaussian processes and Bayesian inference. Dataset. Newcastle University, doi:10.25405/data.ncl.14447670.v2.
- Svalova, A., Helm, P., Prangle, D., Rouainia, M., Glendinning, S. & Wilkinson, D. J. (2021). Emulating computer experiments of transport infrastructure slope stability using Gaussian processes and Bayesian inference. *Data-Centric Engineering* **2**, e12, doi:10.1017/dce.2021.14.
- Yu, Z., Stirling, R., Glendinning, S., Hughes, P. & Brooks, H. (2021). Data from bionics research embankment. Dataset. Newcastle University, doi:10.25405/data.ncl.15506019.